Journal of Sound and Vibration (1995) **179**(1), 13–36

ANALYTICAL SOLUTION FOR MODULATION SIDEBANDS ASSOCIATED WITH A CLASS OF MECHANICAL OSCILLATORS

G. W. Blankenship

General Motors Corporation, *Powertrain Division*, 37350 *Ecorse Road*, *Romulus*, *Michigan* 48174-1376, *U.S.A.*

AND

R. Singh

Acoustics & Dynamics Laboratory, *Department of Mechanical Engineering*, *The Ohio State University*, *Columbus*, *Ohio* 43210-1107, *U.S.A.*

(*Received* 12 *April* 1993, *and in final form* 10 *September* 1993)

Sideband structures are a commonly observed phenomenon in measured vibro-acoustic signatures of many types of mechanical systems, and especially in rotating machinery. Such spectral information is often used for fault diagnostic applications as well as noise and vibration control studies. A new theory is developed that examines in a critical manner the commonly held belief that simple amplitude and frequency or phase modulation processes are responsible for generating such sidebands, and instead provides a more logical explanation. A class of viscosity damped mechanical oscillators is examined having spatially periodic stiffness and displacement excitation functions that are exponentially modulated by the instantaneous vibratory displacement of the inertial element. To this end, a new family of dual domain periodic differential equations is introduced which is shown to be more pertinent to the study of force modulation inherent to many mechanical systems, such as a gear pair. Analytical expressions are then derived to predict sideband amplitudes in terms of key system parameters. The harmonic balance method and direct time domain integration techniques are employed to study various subsets of the problem.

1. INTRODUCTION

Sideband structures are a commonly observed phenomenon in measured vibro-acoustic signatures of many types of mechanical systems and especially in rotating machinery [1–3]. A typical auto-power spectrum of, say, an acoustic pressure or a structural acceleration signal, may contain many low order and high order harmonic components along with complex sideband structures. Such spectral information is often used for noise and vibration control studies [2] as well as fault diagnostic applications [3]. Although the frequency of each harmonic is ultimately related to the kinematics of a mechanical linkage or mechanism, the amplitude characteristics usually result from complex dynamic acoustic processes. The intent of this paper is to unravel some of the unknown aspects associated with a class of mechanical oscillators that exhibit such spectral characteristics. A new theory is developed that examines in a critical manner the commonly held belief that simple amplitude and frequency or phase modulation processes are responsible for generating such sidebands [1, 3].

The genesis of this line of enquiry arises from the study of gear dynamics, in which sideband structures are especially germane to experimental diagnostic studies [1–3]. Based

0022–460X/95/010013 + 24 $8.00/0

on the unique problem of a single gear pair system, a simplified mathematical formulation emerges which could be extended to other physical systems. Accordingly, some of the terminology from the context of gear dynamics is retained for the sake of clarity in mathematical and physical interpretation [4].

Perhaps of more fundamental importance is the set of mathematical problems grouped under the family of ordinary linear differential equations having periodic, time-varying coefficients, such as the Hill or Mathieu equations [5]. Historically, these equations have been of interest because of their inherent applications to engineering and physical sciences. Most mathematical formulations assume a second order, homogeneous differential equation with sinusoidal or piecewise linear variations of the coefficients or system parameters. The independent variable is usually time t and typically only the initial value problem is solved, with an emphasis on the dynamic stability and parametric behavior of the system [5, 6]. The question naturally arises as to whether these equations are sufficiently well defined to describe the spectral characteristics discussed earlier. To this end, a new class of periodic differential equations is introduced, which is later shown to be more pertinent to the study of force modulation inherent to many mechanical systems. A second order inhomogeneous differential equation is written, where the coefficients and forcing function are assumed to be periodic in a spatial or angular variable $\theta(t)$ rather than time. This spatial variable represents the instantaneous position of the inertia element or mass, which is assumed to have a uniform velocity under ideal conditions. However, vibratory deviations of the mass from its ideal uniform motion give rise to dynamic fluctuations in $\theta(t)$ from its nominal value, thus producing a non-linear feedback effect. This gives rise to rather complex spectral characteristics in the steady state forced response; one of the objectives here is to demonstrate this.

2. PROBLEM FORMULATION

Consider the single-degree-of-freedom (SDOF) oscillator shown in Figure 1, having a spatially periodic stiffness function $k[\theta(t)] = k[\theta(t) + 2\pi]$. Of particular interest is the steady state forced response of this system when it is subjected to a time-invariant mean force F acting on the mass and a spatially periodic displacement excitation function $e[\theta(t)] = e[\theta(t) + 2\pi]$ applied in line with the spring as shown. The governing equation of motion for this system is given by

$$mx'' + cx' + k[\theta(t)]x(t) = F + k[\theta(t)]e[\theta(t)] \tag{1}$$

where the prime denotes differentiation with respect to t. The system mass m and viscous damping coefficient c are both assumed to be time-invariant. In order better to describe certain types of force modulation phenomena, the stiffness and displacement excitation

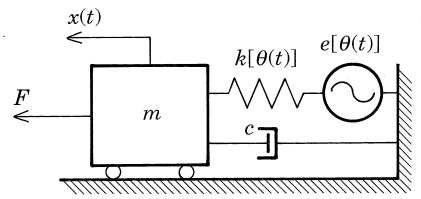

Figure 1. The physical system: a single-degree-of-freedom oscillator having spatially periodic stiffness $k[\theta(t)]$ and displacement excitation (error function) $e[\theta(t)]$ under mean applied load F.

functions in equation (1) are intentionally defined in two distinct analysis domains: the time (t) domain and the spatial (θ) domain. The angular variable $\theta(t)$ is defined as

$$\theta(t) = \Omega t + bx(t), \tag{2}$$

where Ω is a time-invariant mean angular velocity and b is a constant determined by the physical process under study. The second term in equation (2) represents a linear variation in $\theta(t)$ with $x(t)$. Hence, the stiffness and error functions are exponentially modulated by the instantaneous vibratory displacement of the mass. Under such circumstances, b represents the so-called angle modulation depth. For the special case in which $b = 0$, equation (1) is linear with a periodic time-varying stiffness coefficient, and it represents a special class of the forced Hill's equation which has been well studied in various forms [5, 6]. The governing equation is non-linear when $b \neq 0$. The initial value $\theta(t = 0)$ is assumed to be zero in the absence of angle modulation without any loss in generality.

While the right side (r.h.s.) of equation (1) could be replaced with a more general forcing function, it is left in the form given in order to facilitate an investigation of the interaction between the mean force, displacement excitation and stiffness variation which has practical significance to many mechanical system problems. Of particular interest are higher order harmonic components and sideband structures present in the spectra of steady state solutions of equation (1).

The stiffness function $k[\theta(t)] > 0$ is assumed to be positive definite. Furthermore, $k[\theta(t)] = k_0 + k_a[\theta(t)]$ is written as the sum of a time-invariant mean component $k_0 = \langle k \rangle_\theta$ and a spatially periodic alternating component $k_a[\theta(t)]$ with $\langle k_a \rangle_\theta = 0$. A dimensionless time variable $\tau = \omega_n t$ is defined, where $\omega_n = \sqrt{k_0/m}$ is the *static* natural frequency of the system. A dimensionless displacement excitation function $\delta[\theta(t)]$ is defined such that $e[\theta(t)] = E\delta[\theta(t)]$. Here E is some unit displacement amplitude, which is typically of the order of F/k_0. Accordingly, the governing equation (1) can be written in terms of the dimensionless displacement co-ordinate $\xi(\tau) = x(\tau)/E$

$$\ddot{\xi} + 2\zeta\dot{\xi} + \{1 + \alpha\psi[\theta(\tau)]\}\xi(\tau) = f + \{1 + \alpha\psi[\theta(\tau)]\}\delta[\theta(\tau)]. \tag{3a}$$

Here, the dot denotes differentiation with respect to τ, $\zeta = c/2\sqrt{k_0 m}$ is the time-invariant system damping ratio, $f = F/k_0 E$ is the dimensionless mean load and $\alpha\psi[\theta(\tau)] = k_a[\theta(t)]/k_0$, where $\psi[\theta(\tau)] = \psi[\theta(\tau) + 2\pi]$ and $|\psi|_{max} = 1$. Hence, α is a stiffness modulation index and furthermore, $\alpha < 1$ so that the dimensionless stiffness function remains positive definite. The angle parameter $\theta(\tau)$ is now given by

$$\theta(\tau) = \Lambda\tau + \beta\xi(\tau), \tag{3b}$$

where $\Lambda = \Omega/\omega_n$ is a dimensionless frequency ratio and $\beta = bE$ is the dimensionless angle modulation depth.

The scope of this paper is the study of steady state forced response of equations (3) for a viscously damped system with $\beta = 0$ and $\beta \ll 1$. Parameters α and Λ are chosen such that parametric instability issues are not of concern. Consequently, dynamic stability issues are considered only briefly in section 4.1. Various subsets of equations (3) are solved by using both analytical (including the harmonic balance method) and computational approaches. The main emphasis is on the development of analytical expressions which relate sideband amplitudes to key system design parameters, given $\beta = 0$. Since the scope of this enquiry is rather vast, the effect of angle modulation ($\beta \neq 0$) is examined qualitatively in section 6.

3. FUNCTIONAL STIFFNESS AND ERROR EXPRESSIONS

The forced response of the dynamic system considered here is highly dependent upon the explicit forms of ψ and δ. Prior studies have shown that for the linear case ($\beta = 0$), the system behavior is more dependent upon the lower harmonic content of the periodic coefficient ψ and less sensitive to its higher harmonics [5]. Furthermore, the simplest possible forms for ψ and δ are desired which are capable of producing force modulation phenomena which may provide a key to understanding gear dynamics and gear noise. Of great practical interest is the case in which $\psi(\theta) = \psi(N\theta)$ is a high or *mesh frequency* periodic function of $N\theta$, with $N \gg 1$ being a large positive integer and $\delta(\theta)$ being a low or *shaft frequency* periodic function. For example, in a geared system, $\psi(N\theta)$ arises from variations in the number of gear teeth in contact as a function of gear rotation angle θ, $\delta(\theta)$ may represent eccentricity or roundness errors associated with a gear wheel and $\xi(\tau)$ represents the instantaneous relative displacement across the gear mesh interface [4]. Note that $\psi(N\theta)$ has a pumping period of $2\pi/N$, being commensurate with the fundamental excitation period of $\delta(\theta)$ which is of course 2π.

Since the pumping and excitation frequencies are commensurate, the steady state forced response must be periodic with fundamental frequency Λ in the absence of any angle modulation ($\beta = 0$), provided that the system is asymptotically stable [7]. When angle modulation is considered with $\beta \ll 1$, the solution is assumed to remain periodic. In either case, one can readily observe that the steady state forced response will consist of two distinct frequency regimes as shown in Figure 2: (i) The shaft frequency regime and (ii) the mesh frequency regime, which are well separated provided that N is sufficiently large and δ is adequately band limited. Accordingly, $\xi(\tau) = \xi_S(\tau) + \xi_M(\tau)$ can be written as the sum of a shaft frequency component ξ_S and a mesh frequency component ξ_M. The spectral composition of ξ_S is dictated primarily by that of δ and the angle modulation depth β. The spectral composition of ξ_M is considerably more complicated. Even simple harmonic forms of $\psi(N\theta)$ will generate higher order mesh harmonics in ξ_M. Furthermore, the product of $\xi_S(\tau)$ and $\psi(N\theta)$ will generate shaft order sidebands about the respective mesh harmonic components. For this reason, the ξ_M is written as the sum $\xi_M(\tau) = \xi_N(\tau) + \xi_{SB}(\tau)$, where ξ_N contains only the mesh frequency component and its harmonics, while ξ_{SB} contains only sideband frequencies. Angle modulation will induce further harmonic distortion in ξ_N and also contributes significantly to sideband structures given by ξ_{SB}.

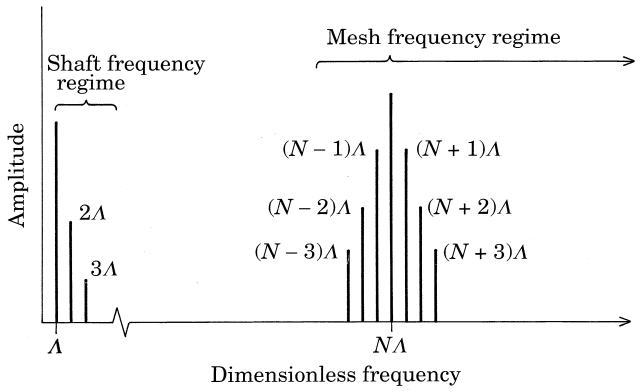

Figure 2. A typical steady state response spectrum illustrating two distinct (shaft and mesh) frequency regimes.

In light of the above discussion, only two simple yet very practical harmonic forms for $\psi(N\theta)$ and $\delta(\theta)$ are considered:

$$\psi(N\theta) = \cos(N\theta), \qquad \delta(\theta) = \Delta_S \cos(\theta + \phi_S), \tag{4, 5}$$

where ϕ_S is a phase angle and Δ_S is a dimensionless displacement amplitude.

4. SOLUTION STRATEGIES

Defining the dimensionless state vector $\mathbf{x}(\tau) = \{\dot{\xi}(\tau) \;\; \xi(\tau)\}^{\mathrm{T}}$, equations (3) are readily cast into the state space form

$$\dot{\mathbf{x}}(\tau) = \mathbf{A}[\theta(\tau)]\mathbf{x}(\tau) + \mathbf{f}[\theta(\tau)], \tag{6a}$$

where $\mathbf{A}[\theta(\tau)]$ and $\mathbf{f}[\theta(\tau)]$ are the time-varying, spatially periodic matrix and forcing vector given, respectively, by

$$\mathbf{A}[\theta(\tau)] = \begin{bmatrix} -2\zeta & -1 - \alpha\psi[\theta(\tau)] \\ 1 & 0 \end{bmatrix}, \qquad \mathbf{f}[\theta(\tau)] = \{f + \{1 + \alpha\psi[\theta(\tau)]\}\delta[\theta(\tau)] \;\; 0\}^{\mathrm{T}}. \tag{6b, c}$$

Equation (6) is linear only when $\beta = 0$. Several methods are available for determining the steady state forced response analytically for the linear case, provided that the system is asymptotically stable. For instance, Struble [8] presents a variational method in which a solution of the form $\xi(\tau) = P(\tau)\cos[N\Lambda\tau + Q(\tau)] + \epsilon\xi_1 + \epsilon^2\xi_2 + \cdots$ is assumed. Here $P(\tau)$ and $Q(\tau)$ are unknown functions that are assumed to vary slowly in time compared with frequency $N\Lambda$. Substituting this assumed solution into equations (6) and collecting terms to the first order yields a set of coupled non-linear differential equations which can be solved for $P(\tau)$ and $Q(\tau)$. However, a general solution is not easily obtained. This method has been employed by Miyasar and Barr [9] to determine the stability of a linear oscillator having a parametric stiffness excitation with externally controlled sinusoidal frequency variation. Another method is to use a harmonic balance type approach by assuming a linear periodic solution and solving for the unknown Fourier coefficients directly. This approach has been widely employed to determine the frequency response of electrical N-networks with time-varying or switched parameter values [10–14]. Since the exact solution contains an infinite number of harmonic terms [15], the approximate solution must be truncated. Hsu and Cheng [7] have also presented an explicit expression for the steady state response of equation (6), given $\beta = 0$ in terms of the fundamental matrix of the homogeneous system, which must also be periodic. The existence of a closed form solution in such cases is dictated by the expression for $\psi(\theta)$. When $\psi(N\theta)$ is a sinusoidal function, the fundamental matrix can be expressed in terms of the well known Mathieu functions [16], but only for specific values of α. Otherwise, the fundamental matrix must be evaluated numerically or by other approximate methods [5, 7].

When $\beta \neq 0$, equation (6) is non-linear and no closed form solutions are known to exist regardless of the expression for ψ. In such cases, equations (6) must be solved by using numerical integration techniques or other approximate methods [8, 17]. However, for $\beta \ll 1$, an approximate solution for $\mathbf{x}(\tau)$ may be obtained by linearizing equation (6) about its static operating point $\mathbf{x}_0 = \{0 \;\; \xi_0\}^{\mathrm{T}}$, where ξ_0 is the *static* solution to equation (3) given $\Lambda = 0$. Here, it is assumed that $\mathbf{x}_0$ does exist and, furthermore, that the solution $\mathbf{x}(\tau)$ is continuous; both assumptions are valid as long as no separation takes place in the physical system. Accordingly, the linearized state equation written in terms of the co-ordinate vector $\mathbf{x}_p(\tau) = \mathbf{x}(\tau) - \mathbf{x}_0$ is obtained by a Taylor series expansion and is given by

$$\dot{\mathbf{x}}(\tau) = \hat{\mathbf{A}}[\theta^*(\tau)]\mathbf{x}_p(\tau) + \mathbf{f}[\theta^*(\tau)]. \tag{7a}$$

Here, $\hat{\mathbf{A}}[\theta^*(\tau)]$ is the linearized coefficient matrix that is periodic in the new spatial parameter $\theta^*(\tau) = \Lambda\tau + \beta\xi_0$ and is given by

$$\hat{\mathbf{A}}[\theta^*(\tau)] = \begin{bmatrix} -2\zeta & -1 - \alpha[\psi(\theta^*) + \psi'(\theta^*)\xi_0] + \psi(\theta^*)\delta'(\theta^*) + \psi'(\theta^*)\delta(\theta^*) + \delta'(\theta^*) \\ 1 & 0 \end{bmatrix}, \tag{7b}$$

where

$$\psi_I'(\theta^*) = -N\beta \sin(N\theta^*), \qquad \delta'(\theta^*) = -\beta\Delta_S \sin(\theta^* + \phi_S). \tag{7c, d}$$

Hence, the static deflection of the system produces a phase shift of magnitude $\beta\xi_0$ in the spatially varying parameters. The angle modulation also gives rise to several additional parametric terms. The products $\psi\delta'$ and $\psi'\delta$ produce apparent stiffness terms at sideband frequencies $(N \pm 1)\Lambda$ and δ' gives rise to an apparent shaft frequency stiffness variation. The number of additional frequencies which must be considered in any analytical solution can become overwhelming when the spectral contents of δ and/or ψ are expanded to include multiple shaft harmonics and/or additional mesh harmonic components.

The steady state solution to equations (7) will be periodic with fundamental frequency Λ due to their linearity. However, as β is increased, the exact governing equation (6) can become strongly non-linear and it may be possible to observe several non-linear phenomena such as period doubling bifurcations and aperiodic behavior [17]; such cases are clearly beyond the scope of this study. No closed form expressions for the fundamental matrix corresponding to either equations (6) or (7) exist for arbitrary values of α, given the assumed forms of ψ and δ. Furthermore, even though it is possible to compute the fundamental matrix numerically in such cases, this may not provide much physical insight. To this end, a modified harmonic balance approach is employed. Analytical solutions are then compared with numerical integration results whenever possible.

4.1. PARAMETRIC RESONANCE AND INSTABILITY

Since the fundamental frequency of $\psi(N\theta)$ is $N\Lambda$, unstable parametric resonance can occur whenever $\Lambda = 2N/\kappa$, where κ is a positive integer [6]. This phenomenon is illustrated in the Strutt diagram shown in Figure 3, which defines regions of instability for $\kappa \leqslant 3$ as a function of α, ζ and Λ/N, given $\beta = 0$. This diagram was obtained by numerically solving for values of α which yield eigenvalues of the monodromy matrix having a modulus equal to unity for given ζ and Λ/N. The monodromy matrix $\mathbf{M} = \mathbf{Z}(2\pi/N\Lambda)$ was determined in the usual manner [6] by solving the homogeneous matrix equation $\dot{\mathbf{Z}}(\tau) = \mathbf{A}(\tau)\mathbf{Z}(\tau)$, given the initial condition $\mathbf{Z}(0) = \mathbf{I}_2$, where $\mathbf{I}_2$ is the 2×2 identity matrix. For viscously damped systems having $\zeta \geqslant 0{\cdot}05$ and $\alpha \leqslant 0{\cdot}6$, the system can only exhibit $\kappa = 1$ instability at frequencies Λ/N greater than about $1{\cdot}72$. In Figure 4 are shown the regions of stable $\kappa = 1$ parametric resonance as a function of α and ζ, given $\Lambda = 2/N$. The boundaries shown in Figure 4 correspond to lines of constant amplitude for the $\Lambda = 1/N$ harmonic component of the normalized steady state forced response $\xi_{ss}(\tau)/f$ obtained by the direct time domain integration of equations (6), given $\Delta_S = 0$. The system was considered to be unstable for $|\xi(\mathrm{j}\Lambda)/f| \geqslant 10$. The lower bound corresponds to $|\xi(\mathrm{j}\Lambda)/f| = 0{\cdot}001$. The actual zone of stable parametric resonance is quite narrow and no parametric resonance corresponding to $\kappa = 1$ occurs for $\zeta \geqslant 0{\cdot}25$ regardless of $\alpha < 1$. In real life, the system response in these unstable regions will be dictated by non-linear effects which are not included in the governing equations given here. However, the focus of this study is on the steady state, non-resonant response, in which any such non-linear effects are typically insignificant.

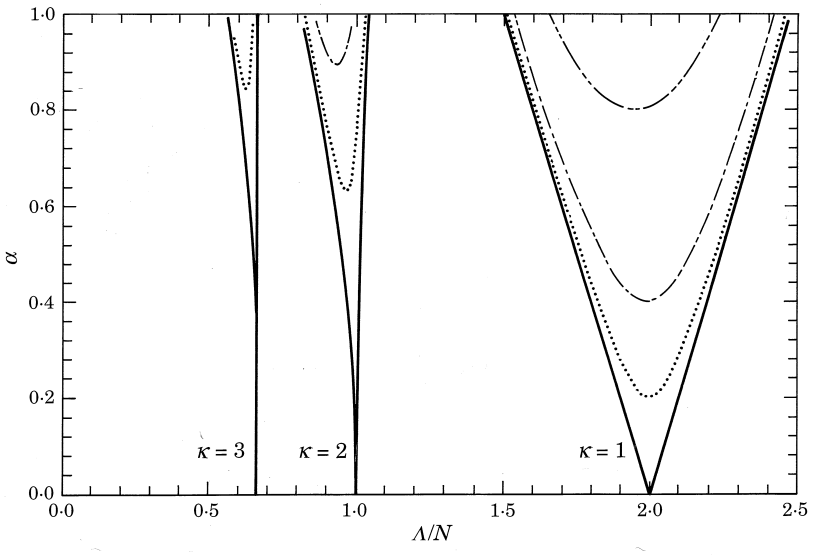

Figure 3. A Strutt diagram, given $\beta = 0$ and $\kappa \leqslant 3$. ——, $\zeta = 0$; · · · ·, $\zeta = 0{\cdot}05$; — · — ·, $\zeta = 0{\cdot}1$; — · · — · ·, $\zeta = 0{\cdot}2$.

When $\beta \neq 0$, the stability of the system can be inferred from equation (7) by examining the eigenvalues of the corresponding monodromy matrix $\mathbf{M} = \mathbf{Z}(2\pi/\Lambda)$, which is determined by solving $\dot{\mathbf{Z}}(\tau) = \tilde{\mathbf{A}}(\tau)\mathbf{Z}(\tau)$ given the initial condition $\mathbf{Z}(0) = \mathbf{I}_2$. Given $N\beta \ll 1$ and $\Delta_S = 0$, the deviation from the stability regions shown in Figure 3 is insignificant. However, as either β or Δ_S becomes large, the regions of instability can vary from those shown in Figure 3. One limiting case occurs when ξ_S is assumed to be zero and θ is exponentially modulated by a harmonic shaft frequency function of the form $\delta(\tau) = \Delta_S \cos(\Lambda\tau + \phi_S)$. Accordingly, the stiffness function $1 + \alpha\psi[\theta(\tau)]$ takes on the form $1 + \alpha \cos[N\Lambda\tau + N\beta\Delta_S \cos(\Lambda\tau + \phi_S)]$. This type of problem has been examined in a more general context by Miyasar and Barr [9]. They found that instability can also occur at frequencies $\Lambda/N = 2N/\kappa(N \pm s)$ where $s = 0, 1, 2, \ldots$ is an integer shaft order index. The

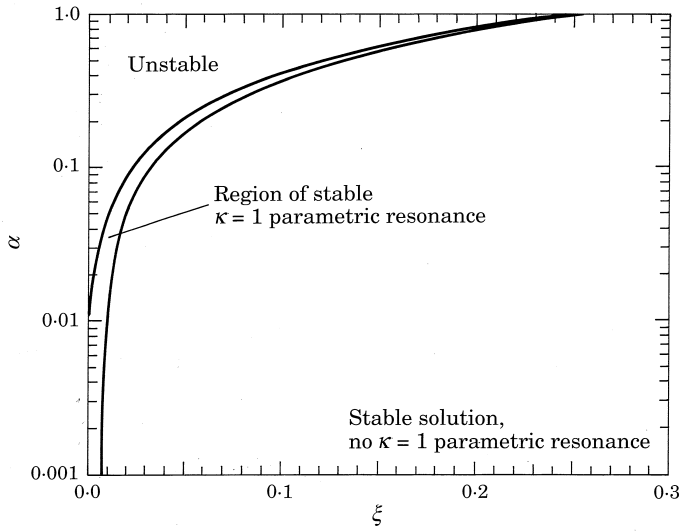

Figure 4. The region of stable $\kappa = 1$ parametric resonance.

region of instability for a given κ becomes an agglomerate of several narrower regions, each associated with one of the above frequencies. The spacing of the individual regions of instability is dictated by the frequency separation ratios $N/(N \pm 1)$. However, for large values of N, the ratios $N/(N \pm 1)$ approach unity and the stability of the system approaches that shown in Figure 3, especially given small values of $N\beta\Delta_S$.

The primary focus of this study is on the steady state response regions in which instability does not occur; such regions are typical of many real-life machines. Accordingly, the remainder of this study considers only values of α and ζ such that the oscillator is operating well outside the stability boundaries shown in Figure 4, given $\Lambda/N < 1{\cdot}8$ or $\Lambda/N \gg 2$. The non-linear oscillator is also assumed to be stable given these conditions; numerical simulation confirms the validity of this assumption.

5. STEADY STATE SOLUTION IN THE ABSENCE OF ANGLE MODULATION ($\beta = 0$)

In this section the governing equation (3) is solved both analytically and numerically, given $\beta = 0$. Several parametric studies are conducted and simplified expressions for the amplitude of the first mesh order sideband pair are developed.

5.1. QUASI-STATIC ANALYSIS

Before proceeding with other exact solutions, a simpler approximate method is first employed to solve equation (3) when $\beta = 0$. This provides physical insight to the role of mean load and stiffness variation on the generation of higher order mesh harmonics. The governing equation can be written exactly in terms of an equivalent *quasi-static loaded excitation function* $\hat{\xi}(f, \theta)$:

$$\ddot{\xi} + 2\zeta\dot{\xi} + \{1 + \alpha\psi[\theta(\tau)]\}\xi(\tau) = \{1 + \alpha\psi[\theta(\tau)]\}\hat{\xi}[f, \theta(\tau)], \tag{8}$$

where $\hat{\xi}(f, \theta)$ may be computed or measured under quasi-static conditions [4] as $\Lambda \to 0$ and is given by

$$\hat{\xi}(f, \theta) = \delta(\theta) + f/[1 + \alpha\psi(\theta)]. \tag{9}$$

The first term of equation (9) represents the original displacement excitation function, while the second term represents an additional displacement arising due to the stiffness variation and is directly proportional to the mean load f. A static compliance function is defined as $[1 + \alpha\psi(N\theta)]^{-1}$ and is plotted versus θ in Figure 5, given $\psi(N\theta) = \cos(N\theta)$ and

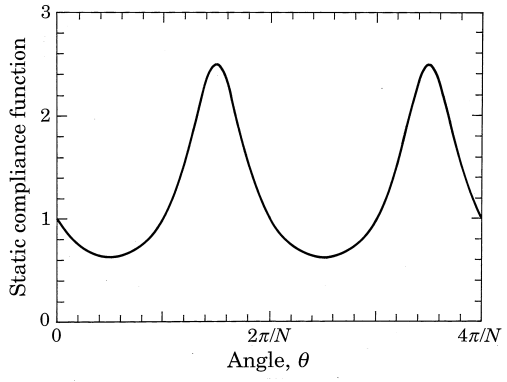

Figure 5. The static compliance function $[1 + \alpha\cos(N\theta)]^{-1}$ *vs.* θ, given $\alpha = 0{\cdot}6$.

$\alpha = 0{\cdot}6$. This compliance function is an even function that is periodic in $N(\theta)$ and can therefore be expressed in terms of the Fourier series

$$[1 + \alpha \cos (N\theta)]^{-1} = \sum_{n=0}^{\infty} a_n \cos (nN\theta), \tag{10a}$$

where n is the mesh harmonic index and Fourier coefficients a_n are given by

$$a_0 = \frac{1}{\sqrt{1-\alpha^2}}, \quad n = 0; \qquad a_n = \frac{2(\sqrt{1-\alpha^2} - 1)}{\alpha^n \sqrt{1-\alpha^2}}, \quad n \geqslant 1 \tag{10b, c}$$

The magnitudes of the first five Fourier coefficients a_0–a_4 are plotted in Figure 6 as a function of stiffness variation α. This simple harmonic stiffness function generates higher order mesh harmonic content in $\hat{\xi}(f, \theta)$, having substantial amplitude for non-zero f when even modest values of α are considered. The mean value of the compliance function also varies with α. However, no sidebands are present in the spectrum of $\hat{\xi}(f, \theta)$. Hence, *displacement sidebands must arise only under dynamic conditions when* $\Lambda \neq 0$, *given* $\beta = 0$.

One obvious simplification of equation (8) is to replace the stiffness term by its spatially averaged mean value to obtain the approximate governing equation

$$\ddot{\xi} + 2\zeta\dot{\xi} + \xi(\tau) = \hat{\xi}[f, \theta(\tau)], \tag{11}$$

which is linear with time invariant (LTI) coefficients only if angle modulation is ignored. The effect of stiffness variation on the system natural frequency is completely neglected in equation (11) and is included implicitly only in $\hat{\xi}$, which is assumed to be available from an independent quasi-static analysis of the oscillator. Equation (11) is particularly convenient when modelling physical systems in which $\hat{\xi}$ can be measured directly. Given the assumed forms of ψ and δ, the steady state solution ξ_{ss} to equation (11) is easily written as

$$\xi_{ss}(\tau) = f/\sqrt{1-\alpha^2} + \Lambda_s M_1 \cos (\Lambda\tau + \varphi_s + \varphi_1) + fM_N(1 - 1/\sqrt{1-\alpha^2}) \cos (N\Lambda\tau + \varphi_N)$$
$$+ f \sum_{n=2}^{\infty} a_{nN} M_N \cos (nN\Lambda\tau + \varphi_N), \tag{12a}$$

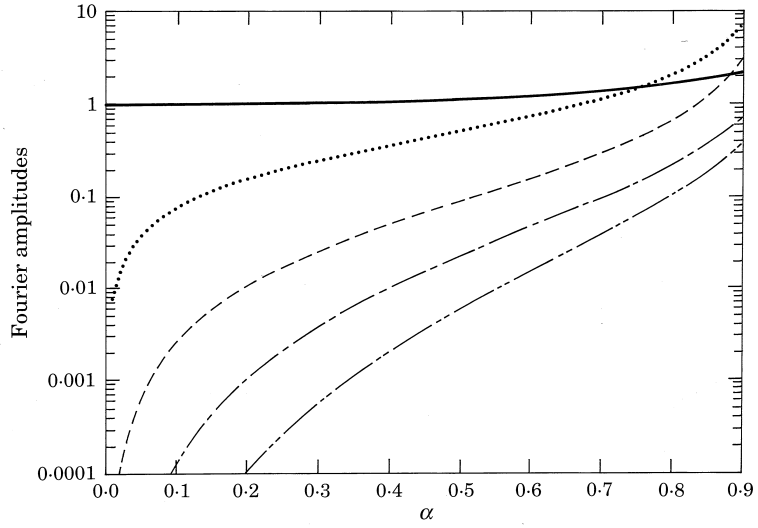

Figure 6. The Fourier amplitudes of the static compliance function $[1 + \alpha \cos (N\theta)]^{-1}$ *vs*. the mesh stiffness variation α. ——, a_0; · · · ·, a_1; – – – –, a_2; — · — ·, a_3; — · · — · ·, a_4.

where M_i and φ_i are amplitude and phase correction factors respectively, given by

$$M_i = \{[1 - (i\Lambda)^2]^2 + 4\zeta^2(i\Lambda)^2\}^{-1/2}, \qquad \varphi_i = \tan^{-1}\left(\frac{2\zeta(i\Lambda)}{1 - (i\Lambda)^2}\right). \tag{12b, c}$$

A typical forced response spectrum showing the normalized peak to peak amplitude of $\xi_{ss}(\tau)/f$ versus mesh frequency ratio Λ/N is shown in Figure 7, given $\Delta_s = 0$, $\alpha = 0{\cdot}4$ and $\zeta = 0{\cdot}10$. Also shown in Figure 7 is the corresponding exact solution obtained by numerical integration of equation (6). Note that the LTI formulation (11) cannot predict the peak at $\Lambda/N = 2$ which arises due to a stable $\kappa = 1$ parametric resonance. Another effect of the stiffness variation is to decrease the apparent natural frequency of the system from its static value of unity. In order to improve the accuracy of the approximate LTI solution, ω_n is replaced by an effective value which is related to the static mesh compliance and is given by $\omega_{neff} = (1 - \alpha^2)^{0{\cdot}25}$. A corrected forced response curve is also shown in Figure 7, which agrees more closely with the exact response for $\Lambda/N \geqslant 0{\cdot}96$, excluding the $\kappa = 1$ parametric resonance at $\Lambda/N = 2$.

In the mesh frequency regime $\Lambda \ll 1$, ξ_S is not affected by α provided that $N \gg 1/(1 - \alpha)$ such that Λ remains well below the lower limit of the instantaneous natural frequency $1 - \alpha$. Furthermore, ξ_S is relatively unaffected by the mesh frequency stiffness variation when the oscillator is operating in the shaft frequency regime $\Lambda/N \gg 1$, provided that N is sufficiently large. This is attributed to averaging effects which occur when the separation between shaft and mesh frequency is large.

The advantage of this approximate LTI solution technique is that it can predict with very reasonable accuracy ξ_S in the appropriate frequency regimes, as well as the peak-to-peak amplitude of ξ_N, with minimal effort. However, the method is incapable of predicting sidebands in the displacement spectrum and the accuracy of individual mesh order amplitudes of ξ_N is relatively poor, as shown later.

5.2. SOLUTION IN THE ABSENCE OF ANGLE MODULATION BY HARMONIC BALANCE

In order to obtain a more accurate closed form expression for the steady state forced response which includes the prediction of modulation sidebands, we employ a modified

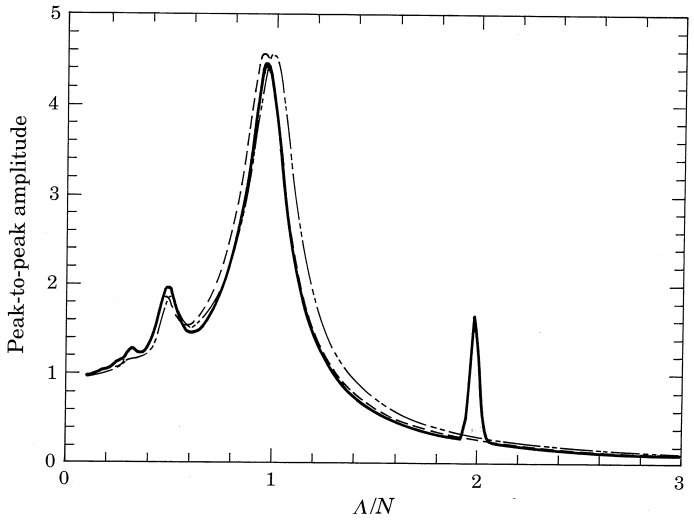

Figure 7. A comparison of the exact solution ξ_{SS}/f (——) and the approximate LTI solutions using $\omega_n = 1{\cdot}0$ (— · · — · ·) and $\omega_{neff} = 0{\cdot}9573$ (· · · ·), given $\Delta_S = 0$, $\zeta = 0{\cdot}1$ and $\alpha = 0{\cdot}4$.

TABLE 1

Frequency mapping of harmonic interactions given $\beta = 0$

Harmonic description	Frequency	Harmonic indices, m
Mean value	0	$0, N$
Shaft order	Λ	$1, N \pm 1$
Lower sidebands	$(nN-1)\Lambda$	$nN-1, (n \pm 1)N-1$
nth mesh order	$nN\Lambda$	$nN, (n \pm 1)N$
Upper sidebands	$(nN+1)\Lambda$	$nN+1, (n \pm 1)N+1$

harmonic balance approach [17]. The following expression for $\xi_{ss}(\tau)$ is assumed:

$$\xi_{ss}(\tau) = \sum_{m=0}^{\infty} A_m \cos(m\Lambda\tau + \gamma_m). \tag{13}$$

Substituting the above expression into equation (3) and collecting even and odd terms of like frequency produces two independent systems of algebraic equations which yield A_m and γ_m when solved. At this point it is instructive to construct the frequency map given in Table 1, which describes the interactions between the various harmonic terms as excited by the assumed forcing functions given $\beta = 0$. Observe that in the absence of angle modulation, the shaft frequency component and sidebands are independent of the mean value and mesh harmonic amplitudes. This makes it possible to perform the respective analyses separately. Letting $a_m = A_m \cos\gamma_m$ and $b_m = A_m \sin\gamma_m$, two independent systems of linear algebraic equations are obtained for shaft–sideband and mesh frequency regimes:

$$\begin{bmatrix}
1-(N\Lambda)^2-\frac{1}{2}\alpha^2 & -2\zeta(N\Lambda) & \frac{1}{2}\alpha & & & & & & \\
-2\zeta(N\Lambda) & (N\Lambda)^2-1 & 0 & -\frac{1}{2}\alpha & & & & & \\
\frac{1}{2}\alpha & 0 & 1-(2N\Lambda)^2 & -2\zeta(2N\Lambda) & \cdot & & & & \\
 & -\frac{1}{2}\alpha & -2\zeta(2N\Lambda) & (2N\Lambda)^2-1 & \cdot & \cdot & & & \\
 & & \frac{1}{2}\alpha & 0 & \cdot & \cdot & \cdot & & \\
 & & & -\frac{1}{2}\alpha & \cdot & \cdot & \cdot & \cdot & \\
 & & & & \cdot & \cdot & \cdot & \cdot & \frac{1}{2}\alpha \\
 & & & & & \cdot & \cdot & \cdot & 0 \\
 & & & & & & \cdot & \cdot & 1-[(m-1)N\Lambda]^2 \\
 & & & & & & & \cdot & -2\zeta(m-1)N\Lambda \\
 & & & & & & & & \frac{1}{2}\alpha
\end{bmatrix}$$

Equation 14 *continued overleaf*

$$
\begin{bmatrix}
-\frac{1}{2}\alpha & & & & & & \\
-2\zeta(m-1)N\Lambda & \frac{1}{2}\alpha & & & & & \\
[(m-1)N\Lambda]^2-1 & 0 & -\frac{1}{2}\alpha & & & & \\
0 & 1-(mN\Lambda)^2 & -2\zeta mN\Lambda & \frac{1}{2}\alpha & & & \\
-\frac{1}{2}\alpha & -2\zeta mN\Lambda & (mN\Lambda)^2-1 & 0 & -\frac{1}{2}\alpha & & \\
 & \frac{1}{2}\alpha & 0 & 1-[(m+1)N\Lambda]^2 & -2\zeta(m+1)N\Lambda & \cdot & \\
 & & -\frac{1}{2}\alpha & -2\zeta(m+1)N\Lambda & [(m+1)N\Lambda]^2-1 & \cdot & \\
 & & & \frac{1}{2}\alpha & 0 & \cdot & \\
 & & & & -\frac{1}{2}\alpha & \cdot & \\
 & & & & & \cdot &
\end{bmatrix}
$$

$$
\begin{Bmatrix}
a_N \\ b_N \\ a_{2N} \\ b_{2N} \\ \cdot \\ \cdot \\ \cdot \\ a_{(m-1)N} \\ b_{(m-1)N} \\ a_{mN} \\ b_{mN} \\ a_{(m+1)N} \\ b_{(m+1)N} \\ \cdot \\ \cdot \\ \cdot
\end{Bmatrix}
=
\begin{Bmatrix}
-f\alpha \\ 0 \\ 0 \\ 0 \\ \cdot \\ \cdot \\ \cdot \\ 0 \\ 0 \\ 0 \\ 0 \\ 0 \\ 0 \\ \cdot \\ \cdot \\ \cdot
\end{Bmatrix}, \tag{14}
$$

$$
\begin{bmatrix}
1-\Lambda^2 & -2\zeta\Lambda & \frac{1}{2}\alpha & 0 & \frac{1}{2}\alpha & 0 & \cdots \\
-2\zeta\Lambda & \Lambda^2-1 & 0 & \frac{1}{2}\alpha & 0 & -\frac{1}{2}\alpha & \cdots \\
\frac{1}{2}\alpha & 0 & 1-[(N-1)]\Lambda]^2 & -2\zeta(N-1)\Lambda & 0 & 0 & \cdots \\
0 & \frac{1}{2}\alpha & -2\zeta(N-1)\Lambda & [(N-1)\Lambda]^2-1 & 0 & 0 & \cdots \\
\frac{1}{2}\alpha & 0 & 0 & 0 & 1-[(N+1)\Lambda]^2 & -2\zeta(N+1)\Lambda & \cdots \\
0 & -\frac{1}{2}\alpha & 0 & 0 & -2\zeta(N+1)\Lambda & [(N+1)\Lambda]^2-1 & \cdots \\
\cdots & \cdots & \cdots & \cdots & \cdots & \cdots & \cdots \\
 & & \frac{1}{2}\alpha & 0 & 0 & 0 & \cdots \\
 & & & -\frac{1}{2}\alpha & 0 & 0 & \cdots \\
 & & & & \frac{1}{2}\alpha & 0 & \cdots \\
 & & & & & -\frac{1}{2}\alpha & \cdots \\
 & & & & & & \\
 & & & & & & \\
 & & & & & &
\end{bmatrix}
$$

$$
\begin{bmatrix}
 & & & & & & \\
 & & & & & & \\
 & & & & & & \\
 & & & & & & \\
\frac{1}{2}\alpha & & & & & & \\
0 & -\frac{1}{2}\alpha & & & & & \\
0 & 0 & \frac{1}{2}\alpha & & & & \\
0 & 0 & 0 & -\frac{1}{2}\alpha & & & \\
\cdots & \cdots & \cdots & \cdots & \cdots & & \\
-[(2N-1)\Lambda]^2 & -2\zeta(2N-1)\Lambda & 0 & 0 & \cdot & & \\
-2\zeta(2N-1)\Lambda & [(2N-1)\Lambda]^2-1 & 0 & 0 & \cdot & \cdot & \\
0 & 0 & 1-[(2N+1)\Lambda]^2 & -2\zeta(2N+1)\Lambda & \cdot & \cdot & \cdot \\
0 & 0 & -2\zeta(2N+1)\Lambda & [(2N+1)\Lambda]^2-1 & \cdot & \cdot & \cdot \\
\frac{1}{2}\alpha & 0 & 0 & 0 & \cdot & \cdot & \cdot \\
 & -\frac{1}{2}\alpha & 0 & 0 & \cdot & \cdot & \cdot \\
 & & \frac{1}{2}\alpha & 0 & \cdot & \cdot & \cdot \\
 & & & -\frac{1}{2}\alpha & \cdot & \cdot & \cdot \\
 & & & & \cdot & \cdot & \cdot
\end{bmatrix}
$$

Equation 15 *continued overleaf-*

$$\begin{Bmatrix} a_1 \\ b_1 \\ a_{N-1} \\ b_{N-1} \\ a_{N+1} \\ b_{N+1} \\ a_{2N-1} \\ b_{2N-1} \\ a_{2N+1} \\ b_{2N+1} \\ . \\ . \\ . \\ . \\ . \\ . \\ . \end{Bmatrix} = \begin{Bmatrix} \Delta_s \cos \phi_s \\ -\Delta_s \sin \phi_s \\ \frac{1}{2}\alpha\Delta_s \cos \phi_s \\ \frac{1}{2}\alpha\Delta_s \sin \phi_s \\ \frac{1}{2}\alpha\Delta_s \cos \phi_s \\ -\frac{1}{2}\alpha\Delta_s \sin \phi_s \\ 0 \\ 0 \\ 0 \\ 0 \\ . \\ . \\ . \\ . \\ . \\ . \\ . \end{Bmatrix}. \tag{15}$$

Each system of equations is governed by a narrow-banded symmetric coefficient matrix and consists of an infinite number of equations which must be truncated before obtaining a solution. The Fourier amplitudes and phase angles are given by $A_m = \sqrt{a_m^2 + b_m^2}$ and $\gamma_m = \tan^{-1}(b_m/a_m)$, respectively.

5.3. MESH ORDER SOLUTION BY USING HARMONIC BALANCE

The mesh harmonic amplitudes A_{nN} of ξ_{SS} are obtained by solving a truncated system of equations (14). These mesh harmonic amplitudes are normalized with respect to the mean force f and are thus dependent solely upon the values of α and Λ. In Figures 8(a) and (b) it is shown that A_N/f and A_{2N}/f converge rapidly to their exact values as the number of equations is increased beyond $m = n$. The exact values of A_N/f and A_{2N}/f were determined from numerical integration of equation (6), given $\alpha = 0{\cdot}4$ and $\zeta = 0{\cdot}1$. Sufficient accuracy is nearly always achieved by letting $m = n + 1$ when solving for A_{nN}. Further analysis reveals that $A_{(n+1)N} \ll A_{nM}$ for $n \geqslant 2$. Hence, higher order mesh harmonics corresponding to large n, if desired, may be determined by using successive iteration techniques. Numerical bounds on truncation error associated with systems of this type can also be determined [15]. Also shown in Figure 8 are the corresponding harmonic amplitudes obtained from the approximate LTI solution given by equation (11) using ω_{neff}. The LTI solution is inadequate for most cases, especially for higher order mesh harmonics with $n \geqslant 2$. Equation (14) presents an extremely efficient method to compute the exact mesh harmonic response of equation (3) in a fraction of the time required by the direct numerical integration method. The mean value A_0 is obtained directly, once A_N and γ_N are known, by

$$A_0 = f - \tfrac{1}{2}\alpha A_N \cos \gamma_N. \tag{16}$$

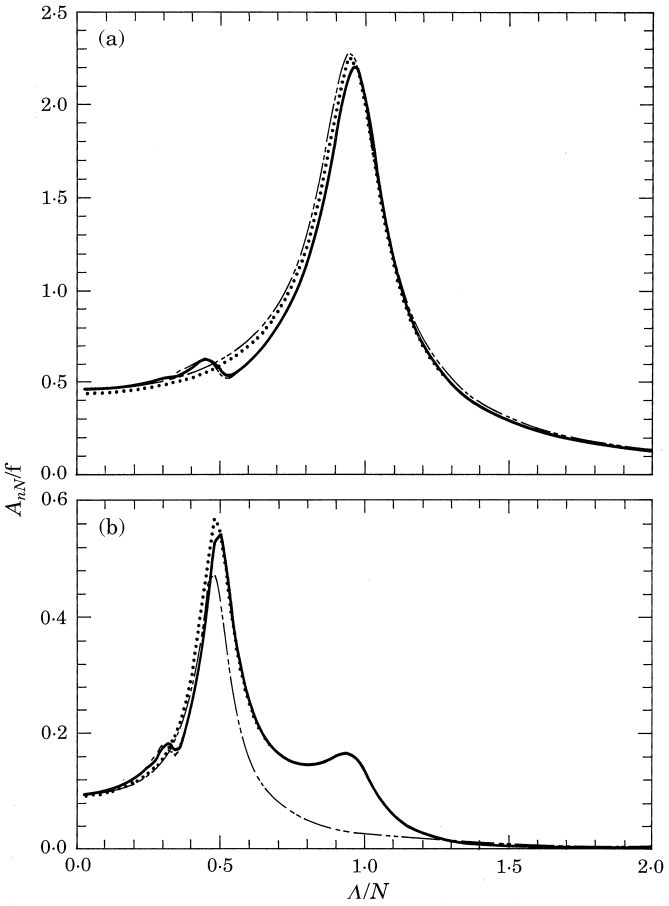

Figure 8. The convergence of the normalized mesh harmonic amplitudes A_{nN}/f obtained by solving equation (15) with $m = n$ (· · ·) and $m = n + 1$ (— · — ·) to the exact value (——), given $\Delta_S = 0$, $\alpha = 0{\cdot}4$ and $\zeta = 0{\cdot}1$. (a) $n = 1$; (b) $n = 2$. — · · — · ·, the corresponding LTI solution.

Also of interest is the total harmonic distortion (*THD*) defined as

$$THD = \sqrt{\sum_{n=2}^{\infty} A_{nN}^2 \Big/ \sum_{n=1}^{\infty} A_{nN}^2}, \tag{17}$$

which serves as an indicator to the significance of higher order mesh harmonic terms given $n \geqslant 2$. The dependence of *THD* on α in the mesh frequency regime is shown in Figures 9(a) and (b), given $\zeta = 0{\cdot}1$ and $\zeta = 0{\cdot}5$, respectively. Note that the *THD* increases with α, especially in the frequency range $\Lambda/N < 1$, and is independent of f. *THD* is not defined for $\alpha = 0$.

5.4. SHAFT–SIDEBAND ORDER HARMONIC BALANCE SITUATION

The shaft and sideband Fourier coefficients of ξ_{SS} are similarly obtained by solving a truncated system of equations (15). Here again, convergence is quite rapid for lower order sideband amplitudes. Numerical investigation of equation (15) reveals that the mesh order stiffness variation has no significant effect on the shaft frequency response regardless of Λ, and in all cases $A_{nN \pm 1} \ll A_1$ regardless of the mesh order index n. Accordingly, the shaft frequency response ξ_S can be determined by a straightforward LTI analysis with no appreciable loss in accuracy; i.e., $A_1 \cong \Delta_S M_1$ and $\gamma_1 \cong \varphi_1$, where M_1 and φ_1 are given by

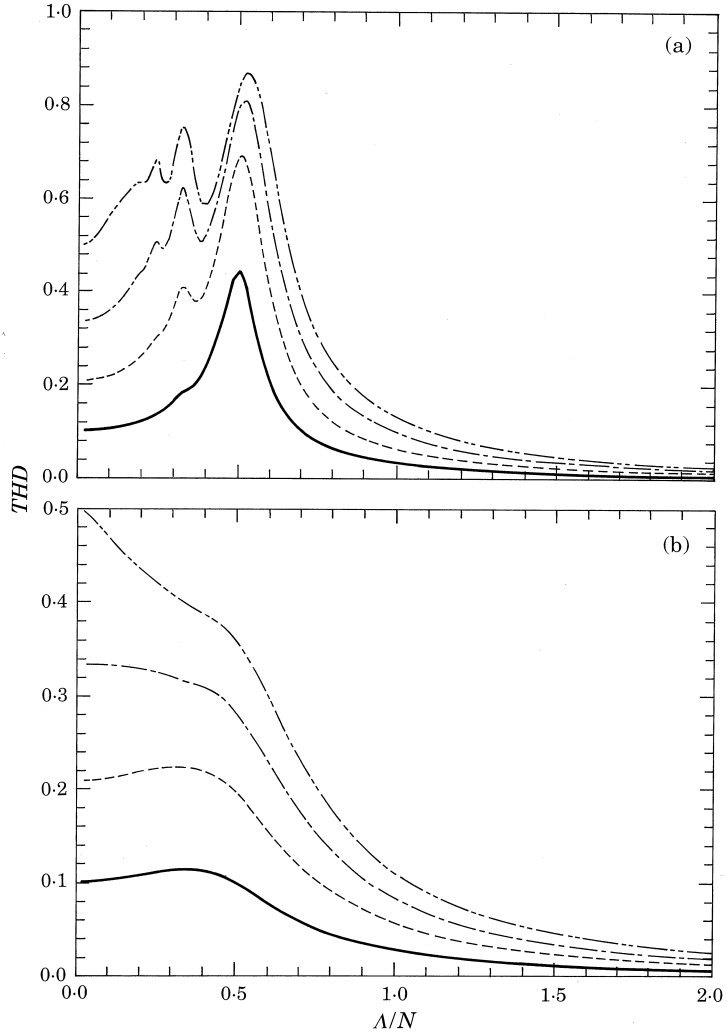

Figure 9. *THD* versus α in the mesh frequency regime, given $\Delta_S = 0$. ——, $\alpha = 0{\cdot}2$; – – – –, $\alpha = 0{\cdot}4$; — · — ·, $\alpha = 0{\cdot}6$; — · · — · · $\alpha = 0{\cdot}8$. (a) $\xi = 0{\cdot}1$; (b) $\zeta = 0{\cdot}5$.

equations (12a) and (12b), respectively. Further analysis shows that $A_{nN\pm1} \ll A_{N\pm1}$ for $n \geqslant 2$ over the entire frequency range, except in some cases near $\Lambda/N = 1/n$ when ζ is very small. In accordance with these assumptions, an approximate solution for the first mesh order sideband pair is obtained by solving equation (15), given $n = 1$:

$$A_{N\pm1} \cong \tfrac{1}{2}\alpha\Delta_S M_{N\pm1} M_1 \sqrt{1 + M_1^{-2} - 2M_1^{-1}\cos\varphi_1}. \tag{18}$$

The above expression provides a reasonably accurate approximation of $A_{N\pm1}$ over the entire frequency range. However, when $\Lambda \ll 1$, $M_1 \to 1{\cdot}0$ and $\cos\varphi_1 \cong 1 - 0{\cdot}5[2\zeta\Lambda/(1-\Lambda^2)]^2$. Accordingly, an even simpler approximation is obtained:

$$A_{N\pm1} \cong \alpha\Delta_S\left(\frac{\zeta\Lambda}{1-\Lambda^2}\right)M_{N\pm1}, \qquad \Lambda \ll 1, \tag{19}$$

which is valid only in the mesh frequency regime, Several observations are made from equations (18) and (19). First, sideband amplitudes are independent of phase angle ϕ_S but, rather, are dictated by the phase correction of the shaft frequency component given by φ_1.

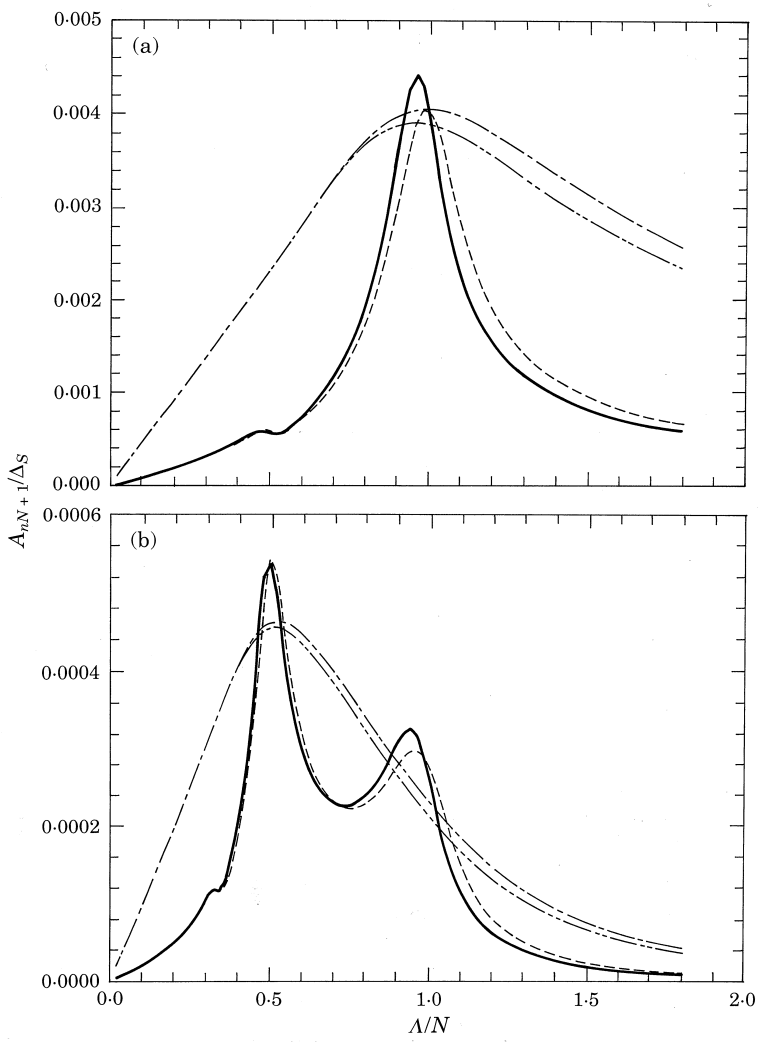

Figure 10. The dependence of normalized sideband amplitudes $A_{nN\pm1}/\Delta_S$ on ζ in the mesh frequency regime, given $\alpha = 0{\cdot}4$ and $N = 50$; A_{nN+1}/Δ_S (——) and A_{nN-1}/Δ_S (– – – –), given $\zeta = 0{\cdot}1$; A_{nN+1}/Δ_S (— · · — · ·) and A_{nN-1}/Δ_S (— · — ·), given $\zeta = 0{\cdot}5$. (a) $n = 1$; (b) $n = 2$.

Hence, sideband amplitudes in the mesh frequency regime in which $\Lambda \ll 1$ are favored by a high damping ratio ζ which induces a larger phase correction at lower operating frequencies; this may be explained as the "broadening" of the resonance around $\Lambda/N = 1$. This phenomenon is clearly illustrated in Figure 10(a), which shows $A_{N\pm1}/\Delta_S$, given $\alpha = 0{\cdot}4$ and $N = 50$ with $\zeta = 0{\cdot}1$ and $\zeta = 0{\cdot}5$ over the mesh range $0 \leqslant \Lambda/N \leqslant 1{\cdot}8$. Higher mesh order sideband amplitudes behave in a similar fashion, as shown in Figure 10(b) for $A_{2N\pm1}/\Delta_S$. These values were obtained by solving equations (15) given $m = 5$, with no significant difference between the corresponding exact solutions obtained by numerical integration. Note the asymmetric in upper and lower sideband pairs $A_{N\pm1}$ which begins to occur near $\Lambda/N = 1/n$. It also follows from equations (18) and (19) that sideband amplitudes in the mesh frequency regime will also favor smaller N. This phenomenon is illustrated in Figure 11, which shows the upper mesh order sideband amplitude A_{N+1}/Δ_S versus Λ/N, given $\alpha = 0{\cdot}4$ and $\zeta = 0{\cdot}1$ with $N = 10$, 50 and 100. Similar trends are observed for higher mesh order sidebands. The accuracy of the approximate solution given by

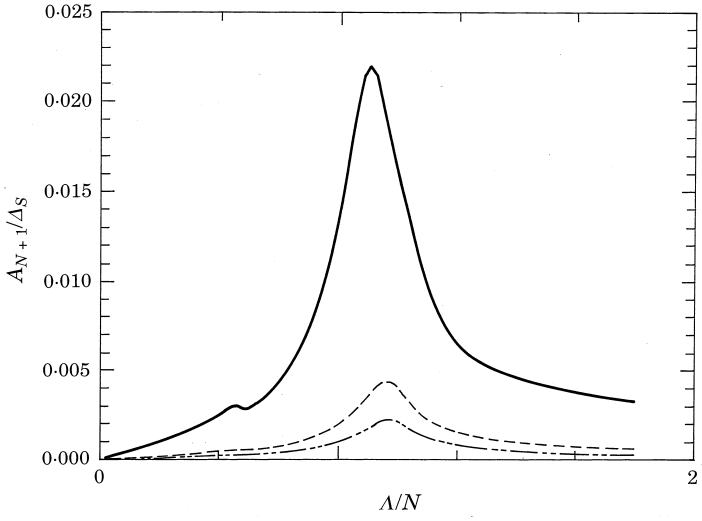

Figure 11. The dependence of the normalized upper sideband amplitude A_{N+1}/Δ_S on N in the mesh frequency regime, given $\alpha = 0{\cdot}4$ and $\zeta = 0{\cdot}1$ ——, $N = 10$; – – – –, $N = 50$; — · · — · ·, $N = 100$.

equation (19) is compared with the exact solution over the mesh frequency regime $0 \leqslant \Lambda/N \leqslant 1{\cdot}8$ in Figure 12, which shows A_{N+1}/Δ_S *vs.* Λ/N given $\alpha = 0{\cdot}4$, $\zeta = 0{\cdot}1$ and $N = 50$. Indeed, equation (19) provides a useful tool to estimate sideband amplitudes.

In the limiting case $\Lambda = 1$, equation (18) reduces to

$$A_{N\pm1} \cong \frac{\alpha\Delta_S}{2(N \pm 1)^2}\sqrt{1 + 4\zeta^2}, \qquad \Lambda \cong 1. \tag{20}$$

Hence, given a large value of N, mesh order displacement sidebands in the shaft frequency regime are relatively small compared to their corresponding values in the mesh frequency regime. This is illustrated in Figure 13, which shows $A_{N\pm1}/\Delta_S$ over the shaft frequency range given $\alpha = 0{\cdot}4$ and $N = 50$ with $\zeta = 0{\cdot}1$ and $\zeta = 0{\cdot}5$. Relative maxima at $\Lambda \cong 1$ occur

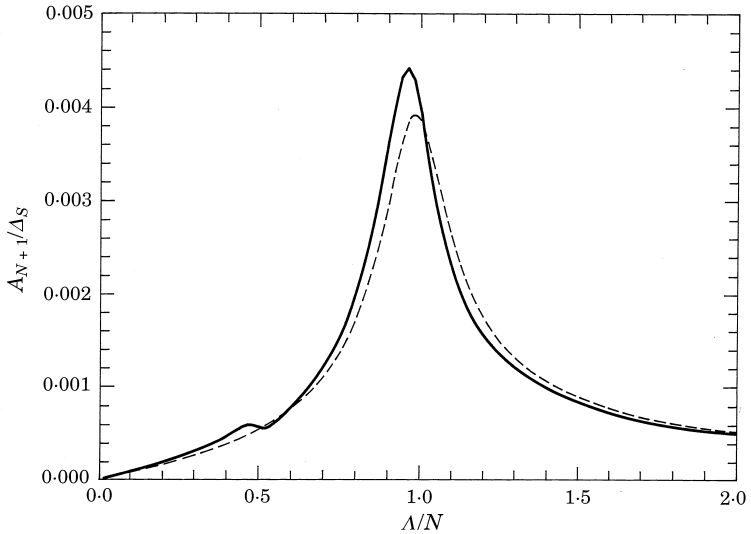

Figure 12. A comparison of the approximate upper sideband solution A_{N+1}/Δ_S (– – – –) given by equation (19) with its exact value (——) in the mesh frequency regime, given $\alpha = 0{\cdot}4$, $\zeta = 0{\cdot}1$ and $N = 50$.

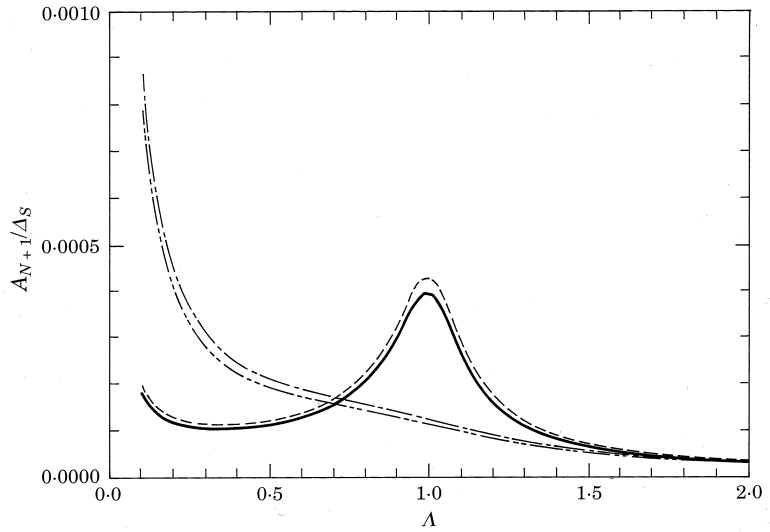

Figure 13. The dependence of the normalized sideband amplitudes $A_{N\pm1}/\Delta_S$ on ζ in the shaft frequency regime, given $\alpha = 0{\cdot}4$ and $N = 50$; A_{N+1} (——) and A_{N-1} (– – – –), given $\zeta = 0{\cdot}1$; A_{N+1} (— · · — · ·) and A_{N-1} (— · — ·), given $\zeta = 0{\cdot}5$.

only for the mesh order sideband pair given small ζ. Higher mesh order sidebands are of negligible amplitude in this frequency range.

5.5. SIDEBAND AMPLITUDE RATIOS

In order to determine whether the amplitude of displacement sidebands is comparable to that of the mesh harmonics, a sideband amplitude ratio (*SBAR*) is defined as

$$SBAR = \sqrt{\sum_{n=1}^{\infty} (A_{nN-1}^2 + A_{nN+1}^2) \Big/ \sum_{n=1}^{\infty} A_{nN}^2}, \tag{21}$$

which can be normalized with respect to Δ_S/f. *SBAR* is found to vary linearly with mesh frequency ratio Λ/N, except for a slight deviation near $\Lambda/N = 1$ for small ζ, as illustrated in Figure 14, which shows $SBAR(f/\Delta_S)$ versus Λ/N, given $\alpha = 0{\cdot}4$ and $N = 50$ with $\zeta = 0{\cdot}05$, $0{\cdot}1$ and $0{\cdot}5$. Furthermore, *SBAR* is directly proportional to ζ/N and is completely

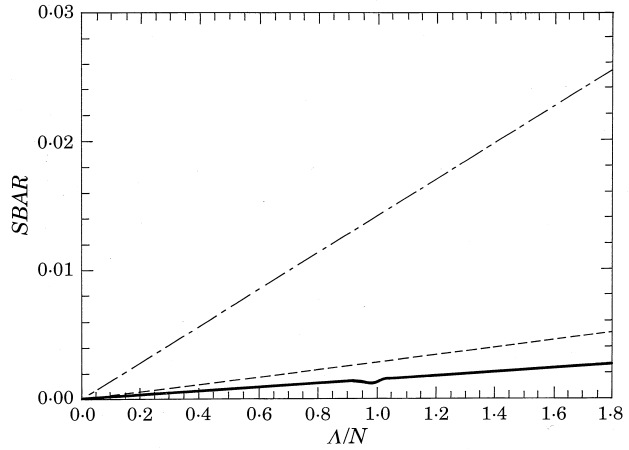

Figure 14. *SBAR* versus Λ/N, given $\alpha = 0{\cdot}4$ and $N = 50$. ——, $\zeta = 0{\cdot}05$; – – – –, $\zeta = 0{\cdot}1$; — · — ·, $\zeta = 0{\cdot}5$.

independent of α. An approximate expression for $SBAR$, valid only for $N \gg 1$ and $\alpha > 0$, is given by

$$SBAR \cong \frac{\sqrt{2}\zeta}{N}\left(\frac{\Delta_S}{f}\right)(\Lambda/N), \qquad N \gg 1, \quad \alpha > 0. \tag{22}$$

$SBAR$ is not defined for $\alpha = 0$. Equation (22) is found to deviate from the exact value of $SBAR$ only near $\Lambda/N = 1$ for very small values of ζ. Typically, $0 < \Delta_S \leqslant 10^4$ and $0 < f \leqslant 10$ for most geared systems. Hence, $0 \leqslant \Delta_S/f \leqslant 10^3$ and, indeed, sideband amplitudes may be of comparable magnitude to the amplitudes of their respective mesh harmonic components. Equation (22) is very useful to determine when sideband components should be included in the calculation of diagnostic and noise perception indices [2].

6. STEADY STATE SOLUTION IN THE PRESENCE OF ANGLE MODULATION ($\beta \neq 0$)

The theory presented in section 5 is capable of predicting only single sideband pairs about harmonics of the meshing frequency due entirely to mesh order stiffness variation and shaft order displacement. However, higher order sidebands having frequencies $(nM \pm s)\Lambda$, where n is a mesh order index and s a shaft order index, are commonly observed in measured vibro-acoustic spectra of many mechanical systems [1–3]. Higher order sidebands $s > 1$ can be predicted given $\beta = 0$ by considering δ to be a periodic function having spectral content to at least order s. Indeed, higher order shaft harmonics in ξ_S are usually observed in spectra exhibiting multiple sideband structures; especially in geared systems. However, in many cases the gear wheel typically does not exhibit any low frequency runout or index errors of order $s > 1$. Another limitation to the theory given $\beta = 0$ is the inability to predict highly asymmetric sideband structures. It is not uncommon to observe differences between corresponding upper and lower sidebands of varying orders of magnitude in measured machinery spectra [1, 3]. However, only relatively small asymmetry can be predicted, given $\beta = 0$. Hence, an alternative explanation is required and the theory is extended accordingly. To this end, angle modulation is introduced via the parameter $\beta = bE$. For example, in a geared system, b corresponds to the reciprocal of the base radius and E is the unit excitation amplitude along the line of action. Typically $10^{-5} \leqslant \beta \leqslant 10^{-3}$ in a geared system.

6.1. SOLUTION DIFFICULTIES

Recall that when $\beta = 0$, $\xi_S(\tau) + \xi_{SB}(\tau)$ is independent of $\xi_N(\tau)$, and it is possible to solve for the mesh and shaft–sideband response independently. Unfortunately, this is not the case, given $\beta \neq 0$, due to strong harmonic interactions which may exist between shaft, mesh and sideband terms depending on the values of N, β and Δ_S. However, given $N\beta \ll 1$ and $\Delta_S\beta \ll 1$, the governing equation (3) can be linearized to yield the state space form given by equations (7), which are sufficiently accurate to model the system behavior given these conditions. The harmonic balance method can be employed to obtain a steady state solution to equation (7), although the system of equations is considerably more complicated. This is evident from Table 2, which illustrates the harmonic interactions given $\beta \ll 1$.

6.2. SOLUTION GIVEN $\Delta_S = 0$

In the case in which $\Delta_S = 0$ and $N\beta \ll 1$, the A_{nN} are easily determined by using equations (14) and substituting α_{eff}, given by

$$\alpha_{eff} = \alpha\sqrt{1 + (N\beta f)^2/(1 - \alpha^2)} \tag{23}$$

TABLE 2

Frequency mapping of harmonic interactions given $\beta \neq 0$

Harmonic description	Frequency	Harmonic indices, m
Mean value	0	$0, 1, N, N \pm 1$
Shaft order	$s\Lambda$	$s, s \pm 1, N \pm (s \pm 1)$
Lower sidebands	$(nN - s)\Lambda$	$nN - s, (n \pm 1)N - s,$ $nN - (s \pm 1), (n \pm 1)N - (s \pm 1)$
nth mesh order	$nN\Lambda$	$nN, nN \pm 1, (n \pm 1)N, (n \pm 1)N \pm 1$
Upper sidebands	$(nN + s)\Lambda$	$nN + s, (n \pm 1)N + s,$ $nN + (s \pm 1), (n \pm 1)N + (s \pm 1)$

in lieu of α. Hence the effect of small β on the steady state response, given $\Delta_S = 0$, is to increase the effective mesh stiffness variation. Of course, the phase must also be adjusted accordingly. Note that α_{eff} is dependent on the mean force f in addition to α and $N\beta$.

6.3. PARAMETRIC STUDY: THE EFFECT OF Δ_S AND β

The steady state response of equation (6), given $\Delta_S \neq 0$ and $\beta \neq 0$, is considerably more complex than that corresponding to $\beta = 0$. No attempt is made here to present an exhaustive study on the effects of angle modulation and a rigorous mathematical treatment of dual domain problems is let for future investigations. Rather, this study is intended only to illustrate the importance of $\beta \neq 0$ and to determine the feasibility of using this new theory is a plausible explanation for observed phenomena. Furthermore, only solutions in the mesh frequency regime are considered. In Figure 15 are shown nine discrete Fourier spectra of $\xi_{SS}(\tau)/f$, given $N = 50$, $\alpha = 0{\cdot}4$, $\zeta = 0{\cdot}1$ and $\Lambda/N = 0{\cdot}8$ with $\Delta_S/f = 1$, 10 and 100 and $\beta = 0$, $0{\cdot}0001$ and $0{\cdot}001$. The phase angle ϕ_S was found not to have any significant effect on the spectral amplitudes and is therefore set equal to zero. The spectra were obtained by transforming steady state solutions of equation (6) from direct time-domain integration. The normalization here is possible only, given $N\beta \ll 1$ and $\beta\Delta_S \ll 1$. An examination of Figures 15 reveals that the effect of β on the displacement spectra is indeed dramatic, even for the very small values of β considered. Increasing the product $\beta\Delta_S$ produces higher order shaft harmonics as well as higher order sideband pairs which may be highly asymmetric. The product $\beta\Delta_S$ has very little effect on lower order mesh harmonic amplitudes provided that $nN\beta\Delta_S \ll 1$, where n is the index of the highest mesh harmonic amplitude of interest. The assumption $\beta\Delta_S \ll 1$ is violated in Figure 15(i) and non-linear effects come into play. There is a large increase in both shaft harmonic and sideband activity, with sidebands having amplitudes equal to or exceeding their corresponding mesh harmonic amplitudes in some cases.

Further numerical investigation reveals that sideband asymmetry is largely a factor of Λ and β. Sidebands also exist under quasi static conditions given $\beta \neq 0$. Most importantly, given $nN\beta\Delta_S \ll 1$, ξ_S is largely independent of ξ_M. However, ξ_M is strongly dependent on ξ_S. Hence, there is a unique one-way dynamic coupling which exists between steady state solutions in the shaft and mesh frequency regimes. This suggests that for certain limiting cases it is possible to solve for ξ_S independently of $\xi_M(\tau)$ and to then employ ξ_S in a separate dynamic analysis in order to solve for ξ_M. This analysis methodology is being pursued by the authors in a companion study to determine analytical solutions for selected

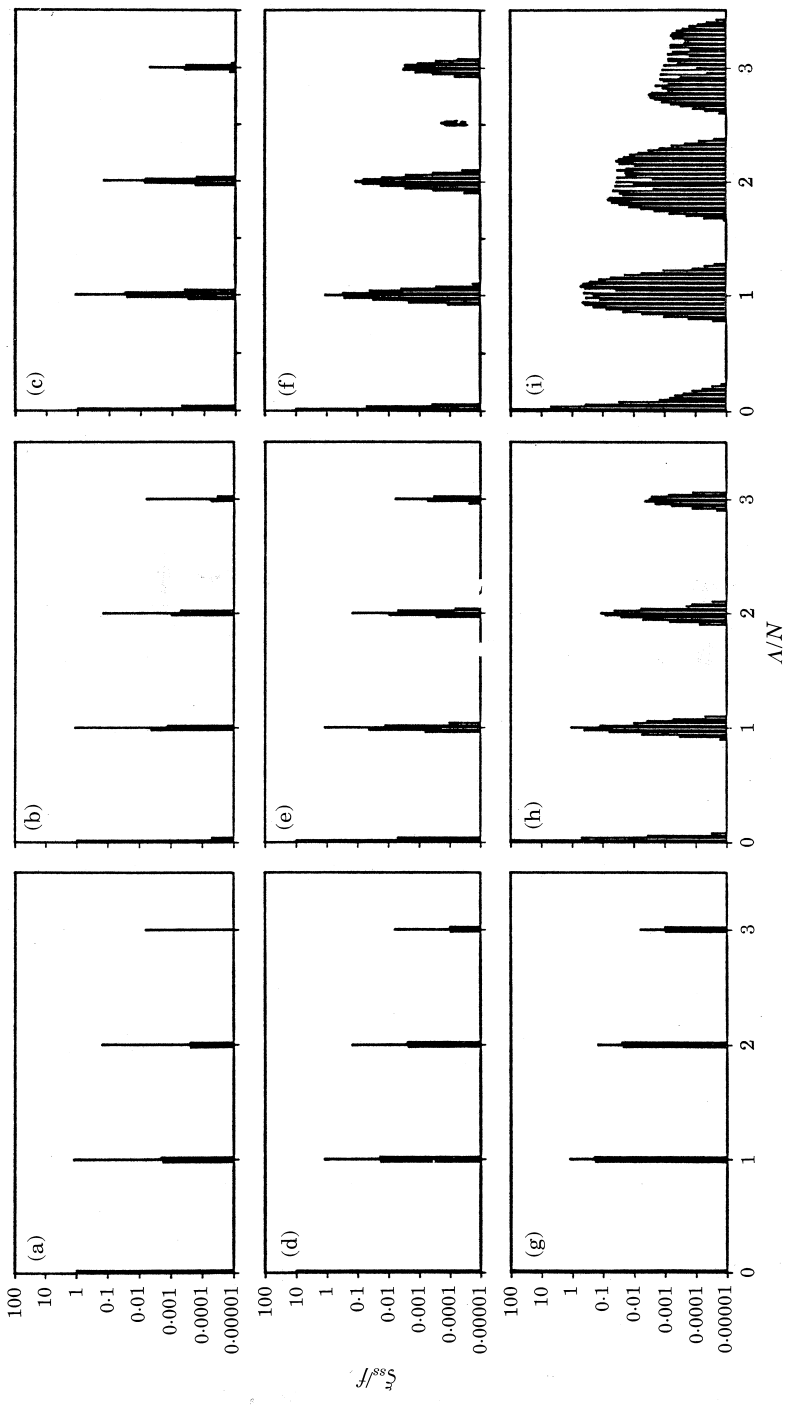

Figure 15. The effect of β on the steady state response spectra of ζ_{ss}/f, given $N = 50$, $\alpha = 0{\cdot}4$, $\zeta = 0{\cdot}1$ and $\Lambda = 0{\cdot}8$. (a–c) $\Delta_s/f = 1$; (d–f) $\Delta_s/f = 10$; (g–i) $\Delta_s/f = 100$. (a, d, g), $\beta = 0$; (b, e, h), $\beta = 0{\cdot}0001$; (c, f, i), $\beta = 0{\cdot}001$.

sideband amplitudes for a class of linear oscillators having an exponentially modulated spatially periodic stiffness term.

7. PRIOR EXPLANATIONS FOR SIDEBANDS BASED ON COMMUNICATION THEORY

Before closing, it is necessary to comment on prior theory offered in an attempt to explain sideband phenomena such as that shown in Figure 15. Many investigators have employed concepts directly from electrical communications theory. In particular, combined amplitude modulation (AM) and frequency (FM) for phase modulation (PM) processes have been proposed as viable explanations for sideband phenomenon in geared systems [3]. Typically, a spatially periodic mesh frequency *carrier* function $x_c[N\theta(\tau)]$ is assumed in conjunction with two independent harmonic, time-varying, shaft frequency AM and FM or PM *message* functions $x_{AM}(\Lambda\tau)$ and $x_{FM/PM}(\Lambda\tau)$. These assumed expressions are combined in the usual fashion [3, 18] to obtain an overall expression for the steady state response $x(\tau)$, which generally takes on a form similar to the expression given below for combined AM and PM:

$$x(\tau) = [1 + \alpha x_{AM}(\Lambda\tau)]\cdot x_c\{N[\Lambda\tau + \beta x_{PM}(\Lambda\tau)]\}. \tag{24}$$

Here, α is an AM modulation index and β is a PM modulation depth. Typically, the AM message function is assumed to be free from any phase modulation effects. While such theory may provide qualitative understanding of various modulation processes and their resultant spectral composition, its effective use as an analysis tool to describe the spectra associated with many types of mechanical systems is limited to certain types of quasi-static PM phenomenon and certain types of AM and PM phenomenon due to external variations in Λ and f [19]. Both Λ and f are assumed to be time-invariant in the present study. Furthermore, conventional modulation theory is often not capable of predicting sidebands having amplitudes comparable to those predicted by using equation (3) when realistic values for α and β are employed. While it is usually possible to decompose any measured spectra containing sidebands into an effective carrier and AM and PM message functions, these functions usually do not carry any physical significance. For these reasons, the authors have abandoned conventional communication theory in lieu of the new theory proposed in this study, which is believed to provide a more plausible explanation for sideband phenomena occurring in many types of mechanical systems.

8. CLOSURE

A class of viscously damped mechanical oscillators is examined having spatially periodic stiffness and displacement excitation functions that are exponentially modulated by the instantaneous vibratory displacement of the inertial element. To this end, a new class of periodic differential equations is introduced which is shown to be more pertinent to the study of force modulation inherent to many mechanical systems. New analytical expressions are derived to predict sideband amplitudes in terms of key system parameters for one limiting case when angle modulation is not present ($\beta = 0$). Under such conditions, sidebands arise only under dynamic conditions and are most prominent in the mesh frequency regime near $\Lambda/N \cong 1$. When angle modulation is present ($\beta \neq 0$), the spectral contents of the steady-state response are considerably more complex. Strong harmonic interactions can occur between shaft, mesh and sideband components.

Although an attempt is made here to study a generic problem with many potential applications to mechanical systems, the reader must realize that only limited information

can be obtained from a single model. Of more importance is the fundamental understanding of the various physical mechanisms which generate modulation sidebands. The new theory challenges the commonly held belief that simple amplitude and frequency or phase modulation processes are responsible for generating such sidebands and instead provides a more logical explanation for sidebands in terms of fundamental physical parameters. This is believed to be a new contribution to the body of knowledge in the general areas of vibration, acoustics and signal processing.

ACKNOWLEDGMENTS

The authors would like to thank the Powertrain Division of General Motors Corporation for supporting this research.

REFERENCES

1. R. H. Lyon 1987 *Machinery Noise and Diagnostics*. Boston: Butterworth.
2. G. W. Blankenship and R. Singh 1992 *Noise Control Engineering Journal* **38**(2), 81–92. New rating indices for gear noise based upoin vibro-acoustic measurements.
3. R. B. Randall 1982 *Transactions of the American Society of Mechanical Engineers*, *Journal of Mechanical Design* **104**, 259–267. A new method of modeling gear faults.
4. G. W. Blankenship and R. Singh 1992 *ASME Proceedings of the Sixth International Power Transmission and Gearing Conference*, *Phoenix*, *Arizona*, DE-Vol. **43-1**, 137–146. A comparative study of selected gear mesh interface dynamic models.
5. J. A. Richards 1983 *Analysis of Time Varying Systems*. New York: Springer-Verlag.
6. R. A. Ibrahim and A. D. S. Barr 1978 *Shock and Vibration Digest* **10**(1), 15–29. Parametric vibration, part I: mechanics of linear problems.
7. C. S. Hsu and W. H. Cheng 1974 *Transactions of the American Society of Mechanical Engineers*, *Journal of Applied Mechanics* **41**, 371–378. Steady-state response of a dynamical systems under combined forcing and parametric excitation.
8. R. A. Struble 1962 *Nonlinear Differential Equations*. New York: McGraw-Hill.
9. A. M. Miyasar and A. D. S. Barr 1988 *Journal of Sound and Vibration* **124**, 79–89. The linear oscillator under parametric excitation with fluctuating frequency.
10. C. A. Desoer 1959 *IRE Transactions on Circuit Theory* **CT-6**, 244–252. Steady-state transmission through a network containing a single time-varying element.
11. A. Fettweis 1959 *IRE Transactions on Circuit Theory* **CT-6**, 252–260. Steady-state analysis of circuits containing a single periodically-operated switch.
12. J. R. MacDonald and D. E. Edmondson 1961 Proceedings of the Institute of Radio Engineers, U.S.A. **49**(2), 453–466. Exact solution of a time-varying capacitance problem.
13. J. V. Adams and B. J. Leon 1967 *IEEE Transactions on Circuit Theory* **CT-14,** 313–319. Steady-state analysis of linear networks containing a single sinusoidally varying capacitor.
14. M. Liou 1972 *IEEE Transactions on Circuit Theory* **CT-19**, 146–154. Exact analysis of linear circuits containing periodically operated switches with applications.
15. I. W. Sandberg 1964 *IEEE Transactions on Circuit Theory* **CT-11**, 195–201. On truncation techniques in the approximate analysis of periodically time-varying linear networks.
16. N. W. McLachlan 1947 *Theory and Application of Mathieu Functions*. Oxford: Clarendon Press. Reprinted New York: Dover, 1947.
17. D. W. Jordan and P. Smith 1987 *Nonlinear Ordinary Differential Equations*. Oxford: Clarendon Press.
18. P. F. Panter 1965 *Modulation*, *Noise and Spectral Analysis*. New York: McGraw-Hill.
19. G. W. Blankenship 1992 *Ph. D. Dissertation*, *The Ohio State University*, *Columbus*, *Ohio*. Analysis of force coupling and modulation phenomenon in geared rotor systems.